Journal of
Applied Remote Sensing

Fractional snow-cover mapping using an improved endmember extraction algorithm

Ying Zhang
Xiaodong Huang
Xiaohua Hao
Jie Wang
Wei Wang
Tiangang Liang

SPIE

Fractional snow-cover mapping using an improved endmember extraction algorithm

Ying Zhang,[a] Xiaodong Huang,[a,*] Xiaohua Hao,[b] Jie Wang,[b] Wei Wang,[a,c] and Tiangang Liang[a]

[a]Lanzhou University, College of Pastoral Agriculture Science and Technology, State Key Laboratory of Grassland Agro-ecosystems, Lanzhou 730020, China

[b]Chinese Academy of Science, Cold and Arid Regions Environmental and Engineering Research Institute, Lanzhou Gansu 730000, China

[c]Institute of Arid Meteorology, China Meteorological Administration, Lanzhou 730020, China

Abstract. We describe and validate an improved endmember extraction method to improve the fractional snow-cover mapping based on the algorithm for fast autonomous spectral endmember determination (N-FINDR) maximizing volume iteration algorithm and orthogonal subspace projection theory. A spectral library time series is first established by choosing the expected spectra information using prior knowledge, and the fractional snow cover (FSC) is then retrieved by a fully constrained least squares linear spectral mixture analysis. The retrieved fractional snow-cover products are validated by the FSC derived from Landsat imagery. Our results indicate that the improved algorithm can obtain the endmember information accurately, and the retrieved FSC has better accuracy than the MODIS standard fractional snow-cover product (MOD10A1). © *2014 Society of Photo-Optical Instrumentation Engineers (SPIE)* [DOI: 10.1117/1.JRS.8.084691]

Keywords: N-FINDR; orthogonal subspace projection; spectral unmixing algorithm; fully constrained least squares.

Paper 14029SS received Jan. 15, 2014; revised manuscript received Apr. 29, 2014; accepted for publication Apr. 30, 2014; published online May 21, 2014.

1 Introduction

Remote sensing technology provides a convenient approach for snow-cover mapping. Traditional optical remote sensing strategy maps snow through the binary image method (i.e., each pixel is identified as snow or no snow). However, this approach ignores the spatial heterogeneity problem caused by objects, such as rock, soil, and/or vegetation other than snow, especially in some regions where the underlying surface types and terrain are complex. A mixed pixel may contain snow, rock, vegetation, and other land cover, whose recorded spectral information is a mixture of various land surfaces.[1] Specifically, for medium and low-resolution imageries, such as the moderate resolution imaging spectroradiometer (MODIS), the lower the resolution, the greater the possibility of different land surface properties being located within a single pixel.[2] Under these circumstances, it is important to unmix the mixed pixels for better quantitative analysis of snow-cover mapping.

Traditional or intelligent classification algorithms (e.g., supervised classification, neural networks, support vector machines) can only detect the snow appearance at the pixel level, thus no subpixel information is retained. Salomonson and Appel proposed a statistical model based on the snow in European and American snow-covered areas that could measure the global fractional snow-covered area (f_{SCA}) on a subpixel scale. However, a serious limitation of this empirical linear regression algorithm is that it is spatially and temporally dependent.[3] Currently, a number of quantitative analysis approaches (e.g., anomaly detection, endmember extraction, and spectral mixture analysis) used for subpixel component analysis for hyperspectral imagery were introduced to MODIS to resolve mixed pixels.[4,5]

*Address all correspondence to: Xiaodong Huang, E-mail: huangxd@lzu.edu.cn

The existing endmember extraction algorithms for hyperspectral imagery mainly include convex analysis and statistical analysis. Boardman et al. proposed an endmember extraction approach based on pure pixel index.[6] Winter found a solution of maximum volume based on dimension reduction called N-FINDR (an algorithm for fast autonomous spectral endmember determination).[7] Recently, endmember extraction based on statistical analysis has developed rapidly. Zare and Gader put forward an endmember extraction method based on the Dirichlet distribution function,[8] and Banerjee et al. proposed an endmember extraction algorithm based on a support vector machine.[9] Geng developed a maximum volume endmember extraction algorithm without the reduction of dimensions. The algorithm can overlook small targets easily, but can preserve abnormal pixels better than the N-FINDR algorithm.[5] However, as MODIS has a limited number of bands and dimensions compared to hyperspectral images, the quantitative analysis methods for hyperspectral images cannot be used directly for MODIS endmember extraction and automatic unmixing.

In this paper, we propose an improved N-FINDR endmember extraction algorithm based on convex theory combined with the idea of orthogonal subspace projection (OSP),[10] which is used for hyperspectral imagery to extract the endmembers for MODIS imagery automatically. Then, we select the most suitable spectra property curves for different land cover types based on prior knowledge to build a spectral library to retrieve f_{SCA} information from MODIS data.

2 Test Area and Data

2.1 *Study Area*

Our study area is in a $30,020\text{-km}^2$ catchment in the northern Qilian Mountains, which are the headwaters of the Hei-he River. The Hei-he River is the second largest inland river in northwest China, with a main stream length of 821 km. The elevation ranges from 2406 to 5343 m. The local climate is mainly controlled by the high-latitude westerly and polar air circulation.[11] The river basin encompasses a large range of elevations, slopes, and vegetation types and thus is suitable for developing a snow-mapping algorithm, especially one that focuses on mixed-pixel unmixing (Fig. 1).

2.2 *Data*

2.2.1 *MODIS data*

MODIS images have been widely used in climate research,[12–14] hydrologic modeling,[15–17] and glaciology.[18] The MODIS daily snow product (MOD10A1), available at 500-m spatial resolution at least twice daily,[19,20] provides two types of snow products in version 5, a binary snow-cover product and a fractional-snow-cover (f_{SCA}) product. The f_{SCA} product is produced based on an empirical relationship between f_{SCA} and the normalized difference of snow index (NDSI).[21] The MODIS surface-reflectance product (MOD09GA) provides an estimation of the surface reflectance, as it would be measured at ground level in the absence of atmospheric scattering or absorption. MOD09GA provides bands 1–7 in a daily gridded L2G product in the sinusoidal projection, including 500-m reflectance values and 1-km observation and geolocation statistics.

In this study, MOD10A1 and MOD09GA are downloaded from the National Snow and Ice Data Center website, with a spatial resolution of 500 m. The MODIS Reprojection Tool is used to conduct the data format conversion, coordinate transformation, and mosaic. The output data of MOD10A1 is fractional snow cover (FSC).[22] The selected bands of MOD09GA are bands 1–7, wherein the fifth band has been removed as bad data.

2.2.2 *Landsat ETM+*

Enhanced Thematic Mapper Plus (ETM+) is a multiband imagery from Landsat-7, which maintains continuous long-term monitoring of global changes on the Earth. Due to the higher spatial resolution of ETM+ images, it can provide the suitable validation dataset for our results. In this study, three

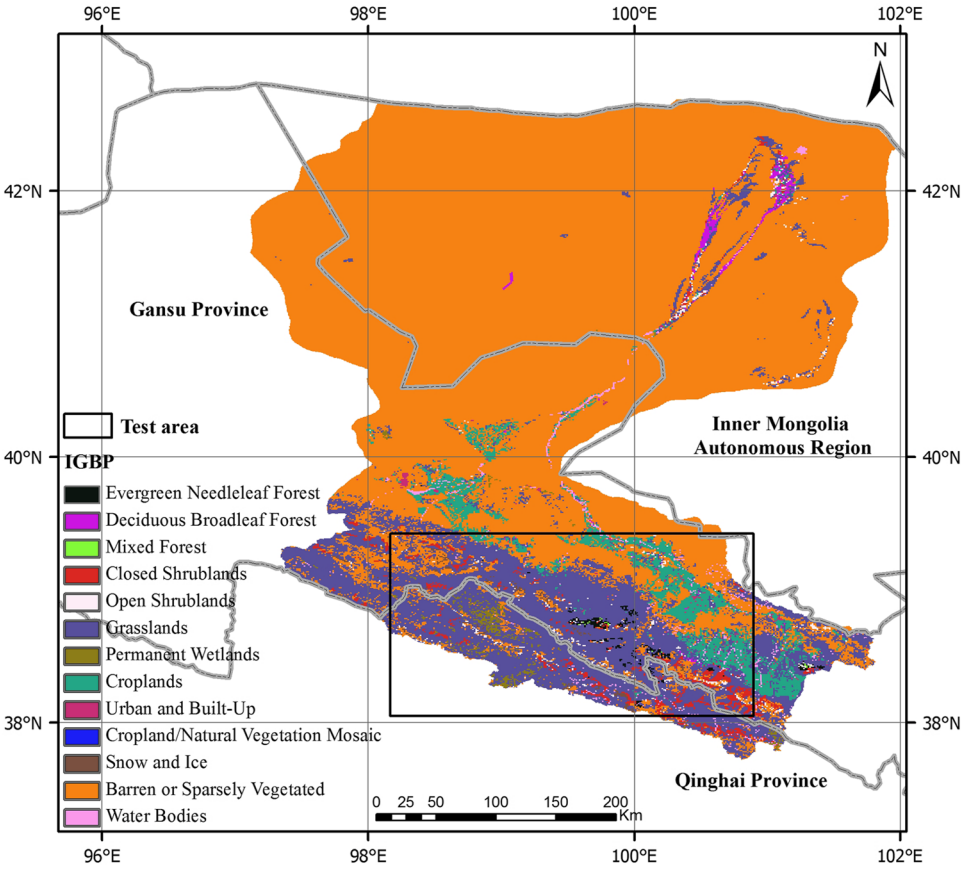

Fig. 1 The International Geosphere–Biosphere Program land cover map of the Hei-he River basin in China in 2011.

cloud-free ETM+ images are used, which were obtained on May 18, 2010, April 3, 2011, and April 28, 2012, respectively. The data gaps in these images are filled by the environment for visualizing images gap fill tools. Taking the snow map retrieved from ETM+ using the SNOWMAP method as the ground truth,[23–26] the f_{SCA} is estimated in each 500-m MODIS pixel by coregistering Landsat ETM+ scenes overlapped with the MODIS pixel and then by summarizing the snow cover in the 30-m ETM+ pixels corresponding to each MODIS pixel.

2.2.3 *IGBP land cover data*

The International Geosphere–Biosphere Program (IGBP)[27] provides crucial data that is used for global change models (e.g., net primary production, ecosystem metabolism models, and carbon cycle models). In this paper, the IGBP land cover data with 500-m resolution in the Hei-he River basin has been used as the prior knowledge for the spectral endmember extraction (Fig. 1). We select five categories of land cover (water, soil, bare land, snow, and vegetation) and cloud cover to build an artificial spectra attribute library for our study area.

3 Methods

3.1 *N-FINDR Algorithm*

N-FINDR (Ref. 7) is an iterative simplex volume expansion approach that assumes in L-spectral dimensions, the L-dimensional volume formed by a simplex with vertices specified by purest pixels (endmembers) is always larger than that formed by any other combination of pixels. N-FINDR finds those vertices by randomly selecting a set of p pixels from the scene as initial endmembers and calculates the volume of the simplex formed by these initial endmembers.

The iterated processes are as follows. First, each of the initial endmembers is replaced one at a time with the pixel being tested. Second, the simplex volumes formed by each replacement are calculated. Finally, the algorithm evaluates if replacing any of the initial endmembers with the pixel being tested results in a larger simplex volume.

Several issues of N-FINDR implementation facilitate the selection of an initial set of endmember pixels for the algorithm. As noted, N-FINDR starts with a random set of initial endmembers that lead to results, which are unrepeatable and inconsistent.

3.2 *Orthogonal Subspace Projection*

The OSP approach has been shown to be a versatile technique for a wide range of applications.[10] OSP signal processing methods have been used to extract the interested spectra. The main concept of OSP is iteration and projection, which can calculate the furthest pixel vector from the average spectrum vector as the endmember and repeat the progress until it obtains all of the vectors. OSP is used to modify the endmember extraction algorithm in this paper.

3.3 *Modified N-FINDR Algorithm with OSP*

Combining N-FINDR with the OSP algorithms, we propose an improved endmember extraction algorithm using a maximizing, volume-based iterative method. First, we set the extracted endmembers to six (representing six categories of soil, water, bare land, snow, vegetation, and cloud, respectively), and then we reduce the dimensions to five (the dimensions equal to the endmembers minus one). Second, we obtain the average spectrum vector of the remote sensing image and calculate the furthest pixel vector from the average spectrum vector as the first endmember e1. Third, each pixel vector of the remote sensing image with e1 is placed in a new array b, and the transpose (b) × b value is then calculated; the transpose (b) represents the matrix transformation of b. We then find the maximum value of transpose (b) × b, and the pixel vector that constitutes the array b is the second endmember e2. Fourth, the first and second endmembers form a new array c with each of the remaining pixel vectors, and we can calculate the maximum value of transpose (c) × c again to obtain the third endmember e3. Finally, a new set of endmembers is produced by iterating the process.

3.4 *Spectral Library Building*

Using the MODIS surface-reflectance product (MOD09GA) combined with the IGBP land-cover map, the maximizing volume iteration algorithm is used to extract the endmembers of six land cover types to acquire the spectrum characteristic curve of those different land cover types; the outlier data are also removed by an artificial examining method. Then, the 10-day spectral library time series based on prior knowledge of the Hei-he basin is built for 2009 (Fig. 2).

3.5 *Subpixel Unmixing Algorithm*

Heinz and Chang developed a fully constrained least squares (FCLS) linear spectral mixture analysis method to obtain the fractional abundances of endmembers. Because no closed form can be derived from this method, an efficient algorithm is developed to yield optimal solutions.[28]

The linear mixture model generally requires two constraints to produce accurate material abundance. These constraints are the abundance sum-to-one constraint and the abundance nonnegativity constraint. The linear spectral mixture model can be represented as follows:

$$P(L) = \sum_{i=1}^{N} c_i e_i + n = Ec + n, \tag{1}$$

$$\sum_{i=1}^{N} c_i = 1, \tag{2}$$

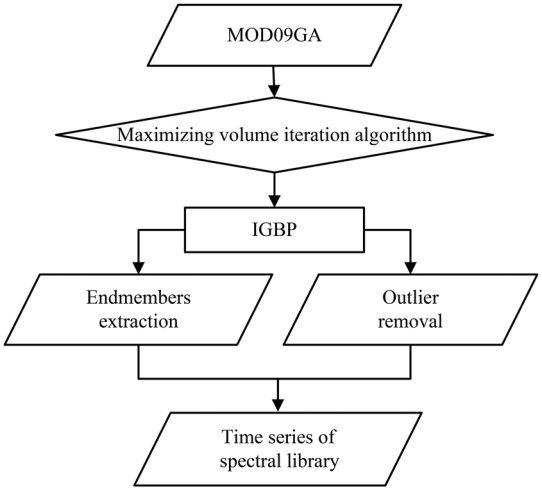

Fig. 2 Flowchart of the spectral library-building method based on prior knowledge.

$$0 \le c_i \le 1, \tag{3}$$

where P is the spectral vector of a pixel, L is the number of spectral bands, and N is the number of endmembers. The c_i represents the fractional abundances of every endmember (e_i) in the pixel vector P. Let E be an $L \times N$ matrix denoted by $[e_1 e_2 \ldots e_N]$, where every column is the endmember vector. Let $c = (c_1 c_2 \ldots c_N)^T$ be a fractional-abundances coefficient vector in the pixel vector P, where n is the noise. Although Eq. (2) is easy to address, Eq. (3) is difficult to implement because it results in a set of inequalities and can only be solved by numerical methods. Consequently, most FCLS-based methods are unconstrained and produce solutions that do not necessarily reflect the true abundance fractions of materials.

In this case, spectral mixture analysis is based on a set of simultaneous linear equations that are solved for the components of the pixel-averaged, atmospherically corrected surface reflectance.[29] In contrast to models that rely on absolute reflectance, this new method uses the relative shape of the snow spectrum. This simultaneous solution from FSC and snow properties is necessary because the spectral reflectance of snow is not just only sensitive to grain size but also to dust or soot content, and organic substances, such as algae and liquid water. Additionally, the spectrum of the mixed pixel is sensitive to the spectral reflectance of the snow fraction.[30–33]

4 Results and Discussion

4.1 *Endmember Screening and Establishing the Spectral Library*

Thirty endmembers are extracted using MOD09GA based on our advanced endmembers extraction algorithm. Then, the most representative six endmembers (representing snow, cloud, vegetation, bare land, soil, and water) from the 30 endmembers, combined with the Hei-he River basin IGBP land-cover data, are screened (Fig. 3). The spectral curve for "bare land" is very different from "soil" because soil typically contains much more water than bare land. In total, 36 10-day interval spectral databases are established throughout the year of 2009 in the Hei-he river basin.

The algorithm takes advantage of maximizing both the volume and dimensionality reduction of the N-FINDR algorithm and also the iterative projection used in the OSP algorithm. Thus, the algorithm increases the computing speed, extracts endmembers that are more representative, avoids the OSP algorithm disadvantage of dimensionality reduction, and overcomes the N-FINDR algorithm weaknesses of unrepeatable volume calculation.

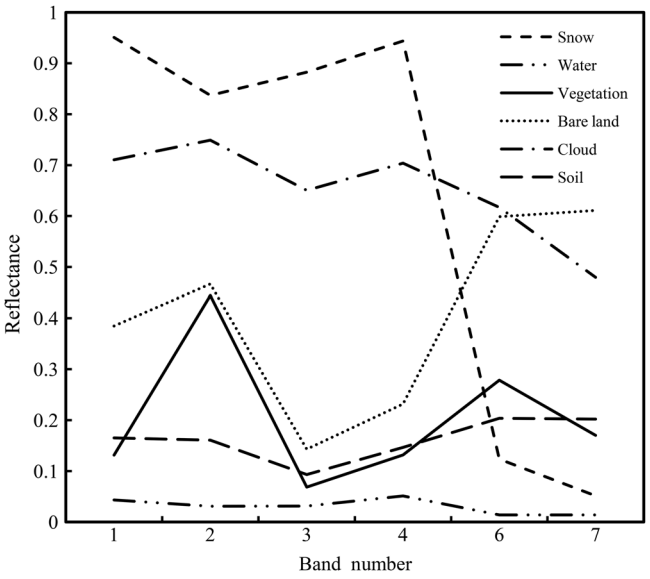

Fig. 3 The reflectance spectral curves of the extracted six endmembers on April 6, 2009.

4.2 *FSC Comparison*

To verify that the established spectral library can be used to produce a more accurate fractional snow-cover map, three snow maps are produced using the FCLS algorithm based on the corresponding time period of the spectral library on May 5, 2010, April 3, 2011, and April 28, 2012 (Fig. 4). The snow maps retrieved from Landsat ETM+ are used as the ground truth to compare with the f_{SCA} product generated by our improved algorithm and with the MODIS standard f_{SCA} product.

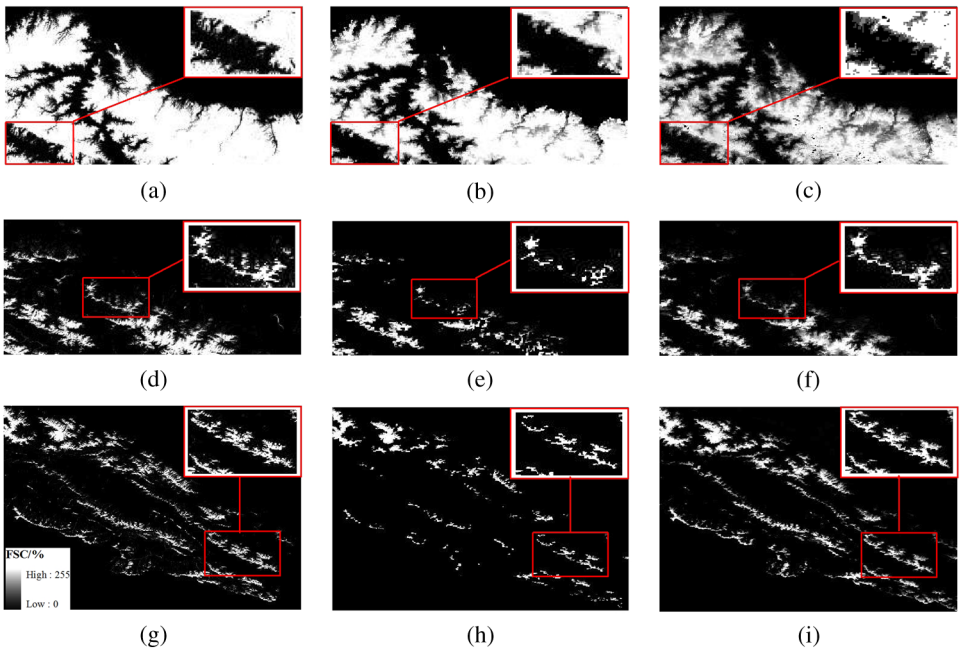

Fig. 4 Snow-cover map comparisons over the upper stream watershed of the Hei-he River basin. (a) Landsat ETM+ snow-cover map on May 18, 2010; (b) MOD10A1 snow-cover map on May 18, 2010; (c) FCLS snow-cover map on May 18, 2010; (d) Landsat ETM+ snow-cover map on April 3, 2011; (e) MOD10A1 snow-cover map on April 3, 2011; (f) FCLS snow-cover map on April 3, 2011; (g) Landsat ETM+ snow-cover map on April 28, 2012; (h) MOD10A1 snow-cover map on April 28, 2012; and (i) FCLS snow-cover map on April 28, 2012.

Table 1 Average FSC from ETM+, MOD10A1, and unmixed FSC products.

FSC (%)	May 18, 2010	April 3, 2011	April 28, 2012	Average
FCLS	48.3	14.2	9.99	24.2
MOD10A1	46.7	8.95	4.06	19.9
ETM+	56.9	27.1	16.7	33.6

Figure 4 shows the f_{SCA} comparisons between ETM+, MOD10A1, and our new product over the three days. The results indicate that the MOD10A1 and FCLS products can identify almost the same snow cover compared to the ground truth, and the FCLS product seems closer to the ETM+ snow products, especially on April 3, 2011, and April 28, 2012. The MOD10A1 fails to retrieve snow in the snow cover-transition areas with patchy snow, while the improved FCLS algorithm consistently maintains its snow retrieval ability in these areas. Table 1 can also support our conclusion. The results show that the ratio of snow-covered area can be retrieved from FCLS, MOD10A1, and ETM+ even though the FCLS f_{SCA} is much lower than the ETM+ but larger than MOD10A1 f_{SCA} for all three days. The results indicate that using the FCLS unmixing algorithm based on endmembers extracted with prior knowledge can improve the snow-cover algorithm of MOD10A1. Specifically, in areas with patchy snow cover, our algorithm can identify more snow cover than MOD10A1.

Table 2 summarizes the basic statistics root mean squared error (RMSE), correlation coefficient (R value), and absolute mean error of the f_{SCA} differences between the two f_{SCA} products and ground truth for the three scenes. For each statistic parameter, the FCLS algorithm shows lower errors and higher correlation coefficient than MOD10A1. The results indicate that MOD10A1 has larger errors compared to the FCLS algorithm over all regions, and our improved FCLS algorithm is feasible to monitor f_{SCA} under a subpixel scale with acceptable accuracy in our study area.

4.3 *Model Sensitivity to Terrain Characteristics*

To determine the sensitivity of the algorithms, we examine the relationship of the fractional errors to the following terrain characteristics: elevation, slope, aspect, and roughness[34] as calculated by the Shuttle Radar Topography Mission DEM V004.[35] Figure 5 shows the mean f_{SCA} errors between two products and ETM+ as a function of elevation, slope, aspect, and roughness in our study area. The results show that terrain characteristics affect the accuracy of fractional snow-cover identification for all the MOD10A1 and FCLS snow products. The errors increase with elevation and reach a maximum at approximately 4500 m and then decrease gradually as

Table 2 Error analysis about MOD10A1 FSC products and unmixed FSC products.

Date	Products	RMSE	R	Absolute average difference
May 18, 2010	FCLS	0.20	0.94	0.23
	MOD10A1	0.23	0.89	0.31
April 3, 2011	FCLS	0.15	0.89	0.17
	MOD10A1	0.53	0.48	0.88
April 28, 2012	FCLS	0.08	0.84	0.17
	MOD10A1	0.13	0.60	0.19
In all	FCLS	0.14	0.89	0.19
	MOD10A1	0.30	0.66	0.46

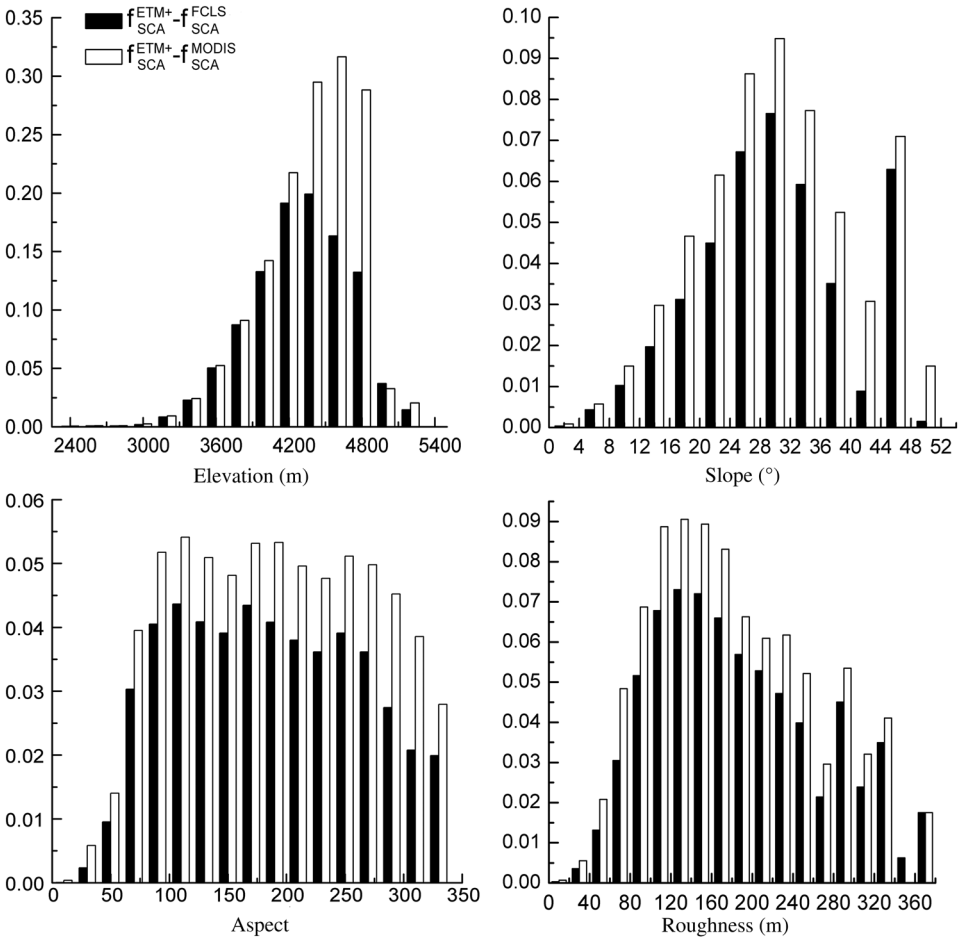

Fig. 5 Absolute error histogram of f_{SCA} as a function of elevation, slope, aspect, and roughness.

elevation increases above 4500 m. Because the terrain surface is relatively flat on the plateau in the study area where the elevation is higher than 4500 m, both the MOD10A1 and FCLS algorithms can extract more snow with higher accuracy. Slope and roughness are two other factors that cause large errors for snow mapping, and our study confirms this observation and shows that the errors increase with slope and roughness but that the relationship becomes uncertain when errors are larger than the threshold. For aspects, the errors increase clockwise from north to south and decrease clockwise from south to north, indicating that more snow can be identified on the back sunny slopes than the sunny slopes because more snow cover accumulates on the north slope and snow on the south slope melts quickly on the plateau. In summary, we observe that elevation is the major factor, while aspect produces the smallest effect among the topographic effects that cause lower accuracy of snow identification; the FCLS algorithm has smaller errors than MOD10A1 under various terrain conditions. Hao et al. found that the standard MODIS snow-cover product has poor accuracy over the Tibetan Plateau mainly due to topographic effects.[36] To improve the accuracy of MODIS snow identification in the mountainous areas, the moderate resolution of optical remote sensing images must be first corrected for topography.

5 Conclusion

This study proposes an improved endmember extraction method to map FSC using a volume-based iterative method that combines the N-FINDER and OSP algorithms. The improved algorithm takes advantage of both maximizing the volume iterative and dimensionality reduction of the N-FINDR algorithm, runs effectively without dimension restrictions, and also retains small targets. The use of the algorithm is an ideal method for extracting endmembers through subpixel

unmixing by establishing a spectral library with prior knowledge; therefore, the algorithm can be used to map FSC on a subpixel scale.

To verify the possibility of using an established spectral library based on prior knowledge of one year to produce f_{SCA} products for other years, the FSC derived from higher spatial resolution Landsat images is used as ground truth to validate the retrieved FSC. The results indicate that the improved algorithm can obtain endmembers accurately and that the established spectral library can be used for measuring subpixel snow cover. Three scenes of f_{SCA} maps retrieved from MOD09GA products are produced in different years using the established spectral library, and three Landsat ETM+ retrieved snow maps are used to validate the f_{SCA} products generated by our improved algorithm. Compared to the MODIS standard f_{SCA} product, our algorithm provides more accurate snow mapping for the study area, especially in the snow-cover edge area because the FCLS algorithm has smaller RMSE and mean errors, but higher R values.

To determine the sensitivity of the algorithms to terrain characteristics, we analyze the influence of different terrain characteristics on our subpixel unmixing algorithm with various elevations, slopes, aspects, and roughness. The results indicate that the terrain characteristics seriously impact the accuracy of snow identification for both MOD10A1 and FCLS algorithms. Although our improved FCLS algorithm performs better and has smaller errors than that of MOD10A1 under various terrain conditions, the topographic effect is the major reason for the low accuracy of snow identification using optical remote sensing data in complex terrain conditions. Therefore, topographic correction before snow mapping could be a possible way to improve the accuracy of MODIS snow identification in mountainous areas.

Acknowledgments

This study is supported by the Chinese State Key Basic Research Project (2013CBA01802), the Chinese Academy of Sciences Action Plan for West Development Project (KZCX2-XB3-15), the National Natural Science Foundation of China (41101337, 31372367, and 31228021), the Fundamental Research Funds for the Central Universities (lzujbky-2013-103), and the Program for Changjiang Scholars and Innovative Research Team in University (IRT13019).

References

1. X. H. Hao et al., "Observations of snow mixed pixel spectral characteristics using a ground-based spectral radiometer and comparing with unmixing algorithms," *Spectrosc. Spectral Anal.* **32**(10), 2753–2758 (2012), http://dx.doi.org/10.3964/j.issn.1000-0593(2012)10-2753-06.
2. J. Wang, *Moderate Resolution Remote Sensing Image Classification, and Target Detect*, pp. 1–3, XinJiang Institute of Ecology and Geography, Chinese Academy of Sciences, China (2011).
3. V. V. Salomonson and I. Appel, "Estimating fractional snow cover from MODIS using the normalized difference snow index," *Remote Sens. Environ.* **89**(3), 351–360 (2004), http://dx.doi.org/10.1016/j.rse.2003.10.016.
4. C. I. Chang, *Hyperspectral Data Exploitation*, pp. 179–201, John Wiley, NewYork (2007).
5. X. R. Geng, *Target Detection and Classification for Hyperspectral Image*, Institute of Remote Sensing Applications Chinese Academy of Sciences, Beijing, China (2005).
6. J. W. Boardman, F. A. Kruse, and R. O. Green, "Mapping target signatures via partial unmixing of AVIRIS data," in *JPL Airborne Earth Sci. Workshop*, Pasadena, California, pp. 23–26 (1995).
7. M. E. Winter, "N-FINDR: an algorithm for fast autonomous spectral endmembers determination in hyperspectral data," *Proc. SPIE* **3753**, 266–275 (1999), http://dx.doi.org/10.1117/12.366289.
8. A. Zare and P. Gader, "Endmember detection using the Dirichlet process," in *Proc. of the IEEE: 19th Int. Conf. on Pattern Recognition*, Tampa, Florida, pp. 1–4 (2008).
9. A. Banerjee, P. Burlina, and J. Broadwate, "A machine learning approach for finding hyperspectral endmembers," in *A Proc. IEEE IGARSS*, Barcelona, Spain, pp. 3817–3820 (2007).

10. Q. Du, R. Hsuan, and C. I. Chang, "A comparative study for orthogonal subspace project ion and constrained energy minimization," *IEEE Trans. Geosci. Remote Sens.* **41**(6), 1525–1529 (2003), http://dx.doi.org/10.1109/TGRS.2003.813704.
11. Y. H. Pan, H. Zhang, and J. Z. Ma, "Quantities research of climate change and human activities affecting water resources," *Yellow River* **34**(5), 55–60 (2012), http://dx.doi.org/10.3969/j.issn.1000-1379.2012.05.019.
12. C. O. Justice et al., "The moderate resolution imaging spectroradiometer (MODIS): land remote sensing for global change research," *IEEE Trans. Geosci. Remote Sens.* **36**(4), 1228–1249 (1998), http://dx.doi.org/10.1109/36.701075.
13. J. R. Dong and C. Peters-Lidard, "On the relationship between temperature and MODIS snow cover retrieval errors in the western US," *IEEE JSTARS* **3**(1), 132–140 (2010), http://dx.doi.org/10.1109/JSTARS.2009.2039698.
14. E. G. Moody et al., "Northern Hemisphere five year average (2000–2004) spectral albedos of surfaces in the presence of snow: statistics computed from Terra MODIS land products," *Remote Sens. Environ.* **111**(2), 337–345 (2007), http://dx.doi.org/10.1016/j.rse.2007.03.026.
15. M. McGuirec et al., "Use of satellite data for streamflow and reservoir storage forecasts in the Snake River basin," *J. Water Resour. Plann. Manage.* **132**(2), 97–110 (2006), http://dx.doi.org/10.1061/(ASCE)0733-9496(2006)132:2(97).
16. T. H. Painter et al., "Response of Colorado River runoff to dust radiative forcing in snow," *Proc. Natl. Acad. Sci. U. S. A.* **107**(40), 17125–17130 (2010), http://dx.doi.org/10.1073/pnas.0913139107.
17. J. Dozier, "Mountain hydrology, snow color, and the fourth paradigm," *Eos Trans. Am. Geophys. Union* **92**(43), 373–374 (2011), http://dx.doi.org/10.1029/2011EO430001.
18. J. Stroeve et al., "Accuracy assessment of the MODIS 16-day albedo product for snow: comparisons with Greenland in situ measurements," *Remote Sens. Environ.* **94**(1), 46–60 (2005), http://dx.doi.org/10.1016/j.rse.2004.09.001.
19. V. V. Salomonson and I. Appel, "Estimating fractional snow cover from MODIS using the normalized difference snow index," *Remote Sens. Environ.* **89**(3), 351–360 (2004), http://dx.doi.org/10.1016/j.rse.2003.10.016.
20. V. V. Salomonson and I. Appel, "Development of the Aqua MODIS NDSI fractional snow cover algorithm and validation results," *IEEE Trans. Geosci. Remote Sens.* **44**(7), 1747–1756 (2006), http://dx.doi.org/10.1109/TGRS.2006.876029.
21. Y. J. Kaufman et al., "Remote sensing of subpixel snow cover using 0.66 and 2.1 μm channels," *Geophys. Res. Lett.* **29**(16), 1781 (2002), http://dx.doi.org/10.1029/2001GL013580.
22. Q. S. Feng, X. T. Zhang, and T. G. Liang, "Dynamic monitoring of snow cover based on MOD10A1 and AMSR-E in the north of Xinjiang Province, China," *Acta Pratacult. Sin.* **18**(1), 125–133 (2009), http://dx.doi.org/10.3321/j.issn:1004-5759.2009.01.019.
23. F. R. Valovcin, "Snow/cloud discrimination," Report A583230, Hanscom Air Force Base, Massachusetts (1976).
24. R. G. Crane and M. R. Anderson, "Satellite discrimination of snow cloud surfaces," *Int. J. Remote Sens.* **5**(1), 213–223 (1984), http://dx.doi.org/10.1080/01431168408948799.
25. J. Dozier, "Spectral signature of alpine snow cover from the Landsat Thematic Mapper," *Remote Sens. Environ.* **28**, 9–22 (1989), http://dx.doi.org/10.1016/0034-4257(89)90101-6.
26. D. K. Hall et al., "MODIS snow-cover products," *Remote Sens. Environ.* **83**(1), 181–194 (2002), http://dx.doi.org/10.1016/S0034-4257(02)00095-0.
27. Z. C. Liu, "IGBP and earth-system," *Arid Land Geogr.* **12**(3), 57–62 (1989).
28. D. C. Heinz and C. I. Chang, "Fully constrained least squares linear spectral mixture analysis method for material quantification in hyperspectral imagery," *IEEE Trans. Geosci. Remote Sens.* **39**(3), 529–545 (2001), http://dx.doi.org/10.1109/36.911111.
29. S. Y. Kotchenova and E. F. Vermote, "Validation of a vector version of the 6S radiative transfer code for atmospheric correction of satellite data, part II: homogeneous Lambertian and anisotropic surfaces," *Appl. Opt.* **46**(20), 4455–4464 (2007), http://dx.doi.org/10.1364/AO.46.004455.
30. S. G. Warren, "Optical properties of snow," *Rev. Geophys.* **20**(1), 67–89 (1982), http://dx.doi.org/10.1029/RG020i001p00067.

31. J. Dozier et al., "Interpretation of snow properties from imaging spectrometry," *Remote Sens. Environ.* **113**(S1), S25–S37 (2009), http://dx.doi.org/10.1016/j.rse.2007.07.029.
32. T. H. Painter et al., "Retrieval of sub-pixel snow-cover, grain size, and albedo from MODIS," *Remote Sens. Environ.* **113**(4), 868–879 (2009), http://dx.doi.org/10.1016/j.rse.2009.01.001.
33. J. Dozier and T. H. Painter, "Multispectral and hyperspectral remote sensing of alpine snow properties," *Annu. Rev. Earth Planet. Sci.* **32**, 465–494 (2004), http://dx.doi.org/10.1146/annurev.earth.32.101802.120404.
34. K. Rittger, T. H. Painter, and J. Dozier, "Assessment of methods for mapping snow cover from MODIS," *Adv. Water Resour.* **51**, 367–380 (2013), http://dx.doi.org/10.1016/j.advwatres.2012.03.002.
35. T. G. Farr et al., "The shuttle radar topography mission," *Rev. Geophys.* **45**(2), RG2004 (2007), http://dx.doi.org/10.1029/2005RG000183.
36. X. H. Hao, J. Wang, and H. Y. Li, "Evaluation of the NDSI threshold value in mapping snow cover of MODIS—a case study of snow in the Middle Qilian Mountains," *J. Glaciol. Geogr.* **30**(1) 132–138 (2008).

Ying Zhang received her Bachelor of Agriculture degree in grassland science from Lanzhou University, China, in 2012. She is currently working toward the MS degree in grassland-geoinformatics at Lanzhou University. Her current research interests include snow remote sensing, snow-cover mapping and modeling.

Xiaodong Huang received a BS degree in geographic information system from the Lanzhou University in 2004, and a PhD degree in grassland science from the Lanzhou University, China, in 2009. Currently, he is associate professor at Lanzhou University. His research interests are in snow cover monitoring using remote sensing technology. Other interests include surface hydrology, agriculture, and environment studies.

Biographies of the other authors are not available.